CHAPTER 3

Greenland Moho Depths from Spectrally Correlated Gravity and Terrain Data

Abstract

The poorly mapped Moho boundary of the Greenland area (58.7 - 84.2° N and 285.75 - 349.50° E) limits the understanding of crustal geologic features and their causative tectonic forces. Seismic estimates of Moho depth model, near surface free-air gravity anomaly observations, and surface elevation and ice thickness data were combined using Gaussian Legendre quadrature integration and correlation analysis to estimate the Moho depths assuming an Airy isostatic model of crustal compensation. The estimated Moho depths compare well (CC=0.95) with 85% of the seismic depth estimates. The derived Moho depth model provides new evidence on the continent-ocean boundary (COB), which suggests that a the continental crust in southwestern Greenland extends up to 100 km further seaward than some current models postulate. The Moho depths are extremely shallow along the coast and deepens further seaward suggesting a coast parallel extension of continental crust. Similar evidence of extension is exhibited along the entire western coast dwindling in magnitude to the north. No evidence for this near coastal extension is observed along the east coast. Spreading centers and transform faults are well identified in the North Atlantic and Baffin Bay, but only weakly identifiable in the Labrador sea region. Additionally, regional features in the root system beneath the South Greenland Archean province have been

identified that may have blocked the progression of volcanism from the regions of Scoresby Sund and Diskó Island into southeastern and southwestern Greenland.

3.1 Introduction

A model of continental and oceanic crustal thicknesses in and around Greenland is important for analyzing the crustal structure and tectonic history of Greenland and can help clarify possible transitions between major lithologic provinces in regions obscured by ice or ocean. In particular, by mapping out the crustal structure, the location of the continent-ocean-boundary (COB) may be enhanced. Kinematic models that describe the opening of oceanic regions rely on the knowledge of the COB to establish current locations for features and to apply rotations to determine starting positions at the time of rifting [Srivastava, 1978; Srivastava and Tapscott, 1986].

Additionally, the origins of some regions, such as the Nares and Davis Straits, are ambiguous. Uncertainty exists as to whether the origin of the Davis Strait and near shore regions of the Labrador Sea are oceanic or continental [Roest and Srivastava, 1989; Gohl and Smithson, 1993]. Debate also continues on the amount of strike-slip motion along the Nares Strait. Geologists indicate only 25 km of movement based upon the displacement of geologic features across the strait, whereas various geophysical models require up to 250 km of displacement [Dawes and Kerr, 1982; Oakey, 1994; Srivastava, 1985]. Improved crustal thickness data also may reveal important new constraints on the presence or possible path of a hotspot under the Greenland region [Lawver and Müller, 1994; Morgan, 1983; Brozena, 1995] related to the Icelandic hotspot, volcanism on Diskó Island and Scoresby Sund, subglacial highlands inferred from the gravity and magnetic anomaly data, and the Alpha Ridge.

Until recently, only relatively sparse coverage of free-air gravity anomalies (FAGA) was available for the interior of Greenland. Coverage was improved dramatically

with the acquisition of aerogravity data at a 30 km nominal track spacing by the Greenland Aerogeophysical Projects of 1991 and 1992 [Brozena, 1995]. These data were incorporated with other marine and surface data by the National Imagery and Mapping Agency (NIMA) to generate a grid of FAGA that was made available for this study.

Enhanced estimates of bathymetry, and hence related estimates of the gravity effects of the rock and ocean masses, are also available [Chapter 2] to complement geologic analyses of the improved gravity coverage. These improved bathymetry estimates were obtained by application of the gravity-geologic method [e.g., Nagarajan, 1994] to satellite altimeter-implied FAGA that are entirely independent of the NIMA FAGA.

In the sections that follow, the application of spectral correlation theory for modeling the Greenland Moho depths and related crustal thicknesses is described. The production of the gravity effects of the ice, rock, and sea water components of the study region are also considered. A model of the Moho depths is produced and checked against seismic and other evidence, and the geologic implications of the estimated Moho depths and crustal thicknesses are also considered.

3.2 Crustal Modeling Methodology

In this study, digital elevation models (DEM) were used to compute grids of the terrain gravity effects (TGE) that, in turn, were combined with a gridded model of FAGA by spectral correlation theory [von Frese et al., 1997] to estimate Greenland Moho depths. DEMs of the ocean, ice, and rock provide a convenient means for estimating the gravitational effect of terrain mass variations by Gaussian Legendre quadrature integration (GLQ) [von Frese et al., 1981]. To calculate the terrain gravity effect (TGE), GLQ integration was applied to prism elements with sides determined

by the DEM grid interval, and top and bottom surface determined by the DEM amplitudes relative to a reference surface.

Each prism was assigned 8 nodes based on the GLQ decomposition of Stroud and Secrest [1966]. These nodes approximate the interval of integration for the entire prism by a summation of densities at the nodes weighted by orthogonal polynomials. In determining the gravitational effects of the prism, these mass nodes emulate in a least squares sense the mass of the entire prism. They are assigned a geographic location and density contrast within each cell, and the cumulative gravitational effect of all of these nodes in all prisms is determined at all grid points for the output gravity grid. The displacement vectors between the nodes and the observation points are fixed from the locations of these points. Hence, the gravity effect determined at a point in the observation grid [von Frese, 1980] may be determined by:

$$\Delta g\left(\phi,\theta,r\right) \approx \Delta\phi_l^{'} \sum_l \left\{ \Delta\theta_j^{'} \sum_j \left(\Delta r_i^{'} \sum_i \left[\left(\frac{G}{l^2}\right) \left(\frac{\partial l}{\partial r}\right) \Delta\sigma \right] A_i \right) A_j \right\} A_l \tag{3.1}$$

where: Δg = the determined gravity effect
(ϕ,θ,r) = the spherical coordinates of Δg (longitude (ϕ), co-latitude (θ), and radial distance (r) from the Earth's center)
$\Delta\phi_l^{'} = \frac{\phi_{la}^{'}-\phi_{lb}^{'}}{2}$
$\phi_{la}^{'}, \phi_{lb}^{'}$ = the lower (a) and upper (b) limits of the l-th coordinate of longitude
$\Delta\theta_j^{'} = \frac{\theta_{ja}^{'}-\theta_{jb}^{'}}{2}$
$\theta_{ja}^{'}, \theta_{jb}^{'}$ = the lower (a) and upper (b) limits of the j-th coordinate of co-latitude
$\Delta r_i^{'} = \frac{r_{ia}^{'}-r_{ib}^{'}}{2}$
$r_{ia}^{'}, r_{ib}^{'}$ = the lower (a) and upper (b) limits of the i-th radial coordinate
G = the universal gravitational constant
l = the linear distance between the source and observation points
$\Delta\sigma$ = density contrast at the source point
A_i, A_j, A_l = tabulated GLQ weights

Assuming appropriate density contrasts for each prism, the TGE were calculated at a 20-km elevation above mean sea level (MSL) to place the calculated gravity

field well above the terrain. This elevation was selected to facilitate estimating the gravity effects of terrain features that have a resolution of about 20-km. This elevation ensured that the spacing between nodes within a prism was smaller than the distance to the observation points at which the effects were being calculated. Also, the limiting resolution of NIMA's FAGA is about 20-km, so that these data could be considered at 20-km altitude without significant loss of anomaly detail. Finally, the programs used to estimate Moho depths limit the size of the solution set such that a 20-km interval of data covers the study region and provides a solution in a reasonable amount of time. Hence, the Moho depth model derived by comparing the TGE and FAGA will also be limited to wavelengths longer than about 20-km.

Gravity analysis always involves ambiguous and non-unique results. However, where the terrain is compensated by crustal thickness, the components of FAGA that are correlated with TGE may reflect the effects of incompletely compensated terrain features. Correlation filters based on the correlation spectrum [von Frese et al., 1997] between FAGA and TGE can be used to separate terrain-correlated (TCFAGA) from terrain-decorrelated (TDFAGA) components in FAGA. Assuming TCFAGA reflect isostatic disequilibrium or dynamically supported topography, they may be removed from the TGE to estimate Compensated TGE (CTGE). The CTGE may then be taken to represent the gravity effects of the crust in equilibrium according to an appropriate model.

The crust in this poorly understood region has been fractured and rotated, which has resulted in smaller blocks and sub-plates [Kerr, 1980; Roest, 1998]. These smaller plates make the selection of an Airy model for isostatic compensation ideal, because of its simplifying features. The CTGE are not visible in the FAGA and hence can be assumed to have an annihilating counterpart (ACTGE) generated possibly by the density contrast at the Moho boundary.

The ACTGE then may be used to estimate the Moho depths by inversion based upon GLQ modeling of lower crustal prisms. In this approach, the mean ACTGE is removed and a reference depth, usually represented by the regional mean depth to Moho boundary, is assumed. Accordingly, variations of the Moho depths about this mean surface are related directly to the variations of the de-meaned ACTGE. Positive values of ACTGE are taken to represent regions of excess mass where the crustal root is shallow and mantle closer to the surface, hence reflecting a positive density contrast. Negative ACTGE values then represent roots deeper than the reference depth and are assigned a negative density contrast. The selection of this reference depth is usually based upon available seismic depth estimates.

Four of the six sides of each prism are again determined by the DEM grid interval. Because either the bottom or top of the Moho depth prism is located at the reference surface, this provides a fifth side. This leaves only the top (where the Moho depth is above the reference depth) or bottom (where the Moho depth is below the reference depth) to be resolved by the inversion.

The final prism surface may be estimated by a least squares inversion if a linear relationship between the mass contained within a prism and the ACTGE field is assumed. The location of the final surface is equivalent to the thickness of the prism either added or subtracted to the reference surface, where the thickness is equivalent to a scale factor multiplied by a unit thickness. Hence, the volume of a prism may be approximated by applying a scale factor to a 1 km thick box with sides determined by the DEM interval. The density contrast within the prism is fixed, hence the mass of the box is also determined by this scale factor. A least squares solution with the ACTGE data will generate the required scale factors assuming *a priori* values of ± 1 km for the thicknesses of all prisms and by altering the radial term ($\Delta r_i' = \frac{r_{ia}' - r_{ib}'}{2}$) in Equation 3.1.

For a prism cell above the reference surface, zero is assumed for the the cell bottom (r'_{ia}) and +1 km for the cell top (r'_{ib}). For a prism cell below the reference surface, -1 km is assumed for the cell bottom (r'_{ia}) and zero for the cell top (r'_{ia}). Implementing these values for r'_{ia} and r'_{ib} in $\Delta r'_i$ yields $-\frac{1}{2}$. The scale factor (S) is then multiplied by this constant value to generate the required $\Delta r'_i$ by:

$$-\frac{1}{2}S = \Delta r'_i = \frac{r'_{ia} - r'_{ib}}{2} = \begin{array}{l} S\frac{0-1}{2} \text{ for cells above the reference surface} \\ = \; S\frac{-1-0}{2} \text{ for cells below the reference surface} \end{array} \tag{3.2}$$

The modified form of Equation 3.1 that takes into account Equation 3.2 is then given by:

$$\Delta g\left(\phi,\theta,r\right) \approx \Delta\phi'_l \sum_l \left\{ \Delta\theta'_j \sum_j \left(-\frac{1}{2} S \sum_i \left[\left(\frac{G}{l^2}\right) \left(\frac{\partial l}{\partial r}\right) \Delta\sigma \right] A_i \right) A_j \right\} A_l \tag{3.3}$$

Since all elements other than the scale factor (S) in Equation 3.3 are constant, it is now linearized:

$$[\Delta g] = [A]\,[S] \;, \tag{3.4}$$

where: $[\Delta g]$ = a vector containing all ACTGE gravity values
$[A]$ = the design matrix related to the constant parts of Equation 3.3
$[S]$ = the desired vector of scale factors

This may be solved using a least squares inversion:

$$\hat{S} = (A^t A)^{-1} A^t \Delta g \tag{3.5}$$

Adjusting the unit prisms by the scale factors determined from the inversion yields the best locations (in a least squares sense) for the Moho boundary with gravity effects that satisfy the ACTGE values. However, the relationship between the nodes and the

observation points is not strictly linear as shown by considering the gravity effects of a prism given by

$$GE = -GM_e \frac{m_{prism}}{l^2} \tag{3.6}$$

where: GE = gravity effect of a prism,
GM_e = the gravitational constant (G) times the Earth's mass (M_e),
m_{prism} = $\Delta\rho$·Volume= $\Delta\rho$·height·width· *length*, and
l = the distance between the source and the observation point

Equation 3.6 is a generalized form for Equation 3.1 and demonstrates that both the mass (m_{prism}) and distance (l) terms are functions of the nodal locations. By increasing the required mass for a prism with a fixed density contrast, the volume must also increase. Because the sides are fixed, the nodes must move vertically with respect to the observation surface, which alters the distance term. If the vertical movement is small with respect to the distance (l), then it can be neglected and the inversion is linearized so that the change in mass is directly proportional to the change in gravity (see Appendix F for a graphical example of this problem). For this case, the node displacement is expected to be as much as 25 km and the distance between the nodes and the observation grid is only 50 km. Clearly then, it will be necessary to iterate this solution as a series of successively closer approximations to the final grid.

Accordingly, initial values of ACTGE are used to generate a first estimates of Moho depths. Using GLQ integration, these estimates are used to calculate a Root Gravity Effect (RGE) that is removed from the ACTGE to generate residuals, which represent the amount of error due to the initial Moho depth model. This process is repeated with the residuals to update the original Moho depth model. The best fit Moho depth model is determined when no further significant improvements in the residual ACTGE values can be determined. Generally, about three iterations were

required to achieve this best fit when experimenting on smaller test cases (i.e., with a 64 by 64 set of observations and a 64 by 64 set of unknowns).

The available seismic depth data (Table E.1 and Figure E.3) and density contrast information determined from previous studies can also be incorporated as constraints. These data will generate fixed scale factors ($\breve{S}_2$) for prisms in areas where these data are available. These fixed scale factors are a subset of the total vector of scale factors ($[S] = [S_1, S_2]$). The unknown scale factors (S_1) are then estimated by:

$$\hat{S}_1 = N_{11}^{-1} A_1^t (\Delta g - A_2 \breve{S}_2) \tag{3.7}$$

where: $\hat{S}_1$ = the remaining unknown depths
N_{11}^{-1} = the inversion matrix $(A_1^t A_1)^{-1}$)
A = the design matrix and its two components $[A_1, A_2]$
Δg = the observation vector
$\breve{S}_2$ = the constraints

The assumed rock densities used initially (Figure 3.16) differentiated only for oceanic and continental regions. After the best fit Moho depth model was obtained using density contrasts derived from these, the Moho depths were fixed and the density contrasts were adjusted to reduce the residual ACTGE values further. This procedure resulted in a hybrid cross of the Airy and Pratt-Hayford isostatic models in the determination of the final Moho depths. Hence, the density in each prism graded from lower density at the surface boundary (rock/air) to higher density inferred at the Moho boundary (crust/mantle), and the density between prisms graded from regions of lower density continental crust to higher density oceanic crust.

Inversion errors may result from incorrect assumptions regarding the terrain densities in the TGE calculations, the densities at the Moho boundary in the ACTGE calculation, and the reference depth. As mentioned above, the reference depth may be adjusted by checking the predictions against the seismic depth estimates. Errors in densities assigned to the contrast at the Moho boundary can be mitigated

by further iterative modification of initial values to reduce residual ACTGE values. Finally, errors in the densities assigned to rock prisms of the terrain are assumed to be sufficiently small for purposes of calculating a regional effect.

Improved densities determined by future investigations for the study region can be readily incorporated to update Moho depth estimates simply by modeling the related gravity effects using the contrast between the old and new densities and adding them to the appropriate gravity fields. Errors in the estimated Moho depths also will reflect errors in the terrain data and FAGA. The next section describes the properties of these data sets for the Greenland study region.

3.3 Data Description

To compute the effective TGE for the terrain analysis, data on glacial thickness, rock topography, and ocean depths were assembled. The ice thickness model is derived from available surface and subglacial DEMs for the Greenland field area only. Bathymetric DEMs were developed by adaption of the Gravity-Geologic Method [Nagarajan, 1994]. Bedrock values in subglacial regions were derived from the Greenland subglacial model.

3.3.1 Ice Thickness Model

The ice thickness model was derived from two Danish DEMs of orthometric heights (heights above the geoid). Figure 3.1 shows the location of the ice and rock surfaces from a surface DEM [Ekholm, 1996], whereas Figure 3.2 shows the bedrock surface beneath the ice from a subglacial DEM [Sohn and Csathó, 1998; Brozena, 1995; Gudmandsen, 1970; personal communication with S. Ekholm, 1998]. The surface DEM, with an average resolution of 2 km, was derived from ERS-1 and Geosat satellite altimetry, and airborne radar and laser altimetry for the ice covered regions. For the

ice-free regions, photogrammetric and manual scans of maps were used to determine elevations. Overall accuracies for the ice-free regions have been shown by Ekholm [1996] to range from 25-35 m for photogrammetrically scanned areas to 200-250 m for the manually scanned areas, while the average accuracy for the ice sheet elevations was 12-13 m. This provides a reasonable level of accuracy for estimating the TGE at the 20-km resolution and elevation for the purposes of this study.

The unpublished subglacial topography model was gridded by Ekholm [personal communication, 1998] from radar soundings made in the 1970's by Gudmandsen [1970] and is much more poorly established than the surface DEM [Brozena, 1995]. The original data were provided in a 5'N by 10'E grid by the Danish Cadastre and Survey (KMS) to Sohn and Csathó [1998] that is comparable to the 6'N by 15'E grid selected for this study. The original tracklines for the soundings were at 30- to 60-km spacings and very sparse in the northern regions [Brozena, 1995]. The resulting subglacial grid was heavily filtered to remove the trackline effects.

The top and bottom of each grid cell are then determined by the two DEMs (Figures 3.1 and 3.2), because they mark the boundary of the ice masses whose gravity effect is to be modeled using GLQ integration. The ice thickness model that is not fixed to any reference surface is shown in Figure 3.3. Regions containing no ice would have the same elevation value in both Figure 3.1 and Figure 3.2. Hence subtracting Figure 3.2 from Figure 3.1 nullifies the ice-free areas and determines the thickness of the ice in subglacial regions.

The surface and subglacial DEMs shown in Figures 3.1 and 3.2 were used for this study. Another surface DEM [Bamber et al., 1997] was developed recently from ERS-1 altimetry but was not available for this study. A surface DEM was also constructed by NASA's GSFC from satellite altimetry [NSIDC, 1997]. However, it shows difficulties in representing regions near the edges of the ice sheet where the altimeter began

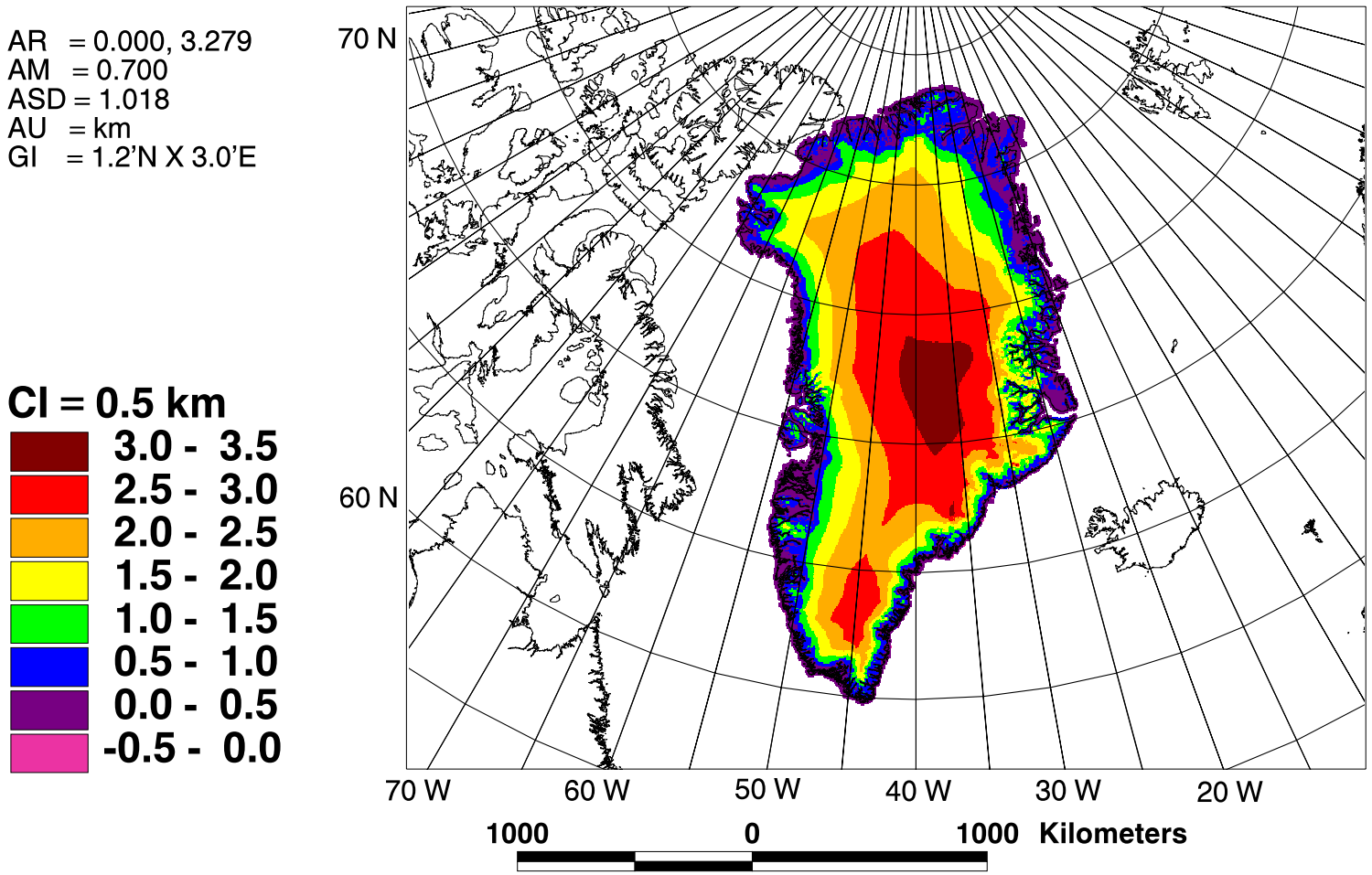

Figure 3.1: Greenland surface elevations including rock and ice surfaces above sea level in a Lambert Equal-Area Azimuthal Projection centered on 40° W.

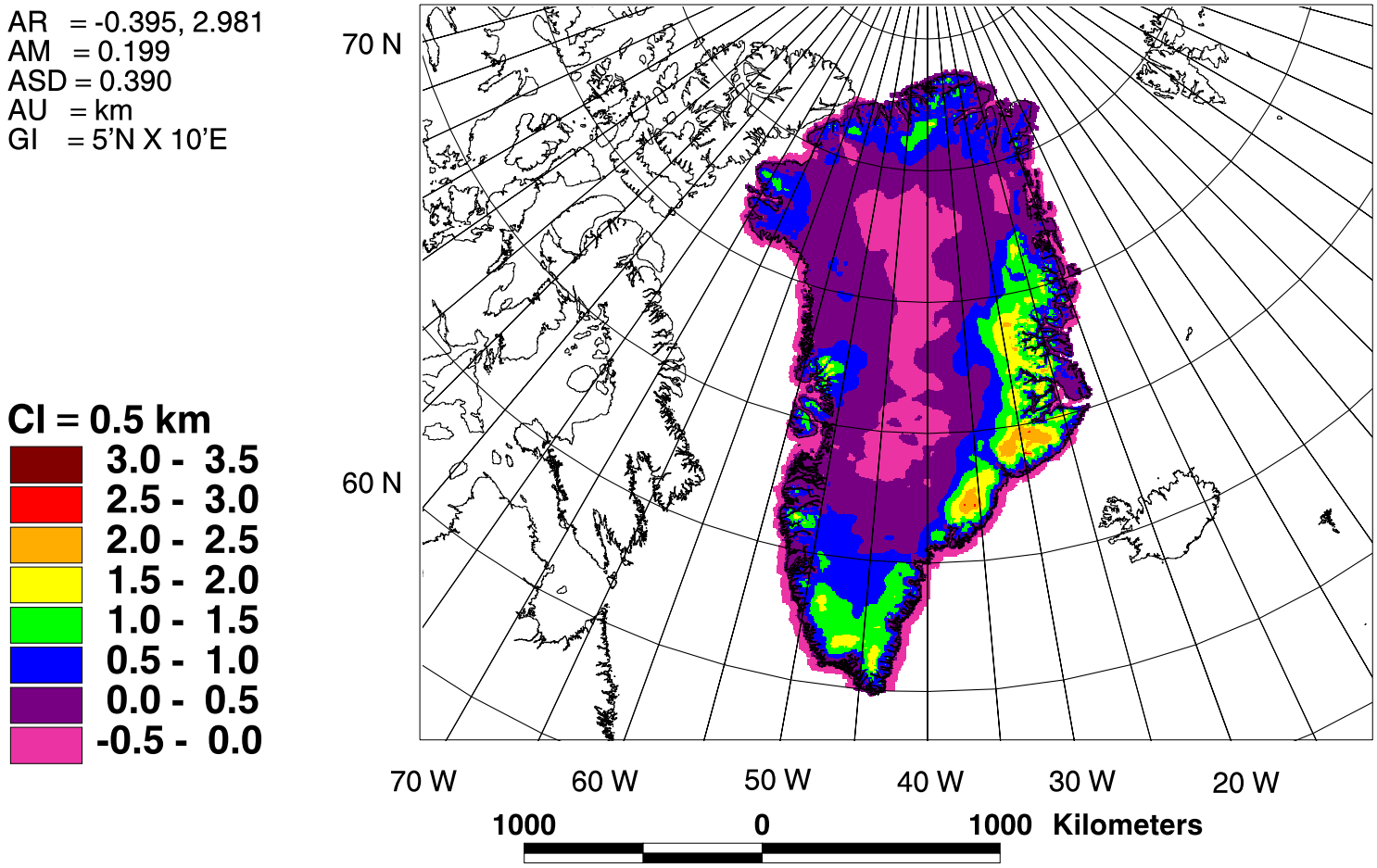

Figure 3.2: Greenland subglacial elevations inferred for the bedrock relative to mean sea level in a Lambert Equal-Area Azimuthal Projection centered on 40° W.

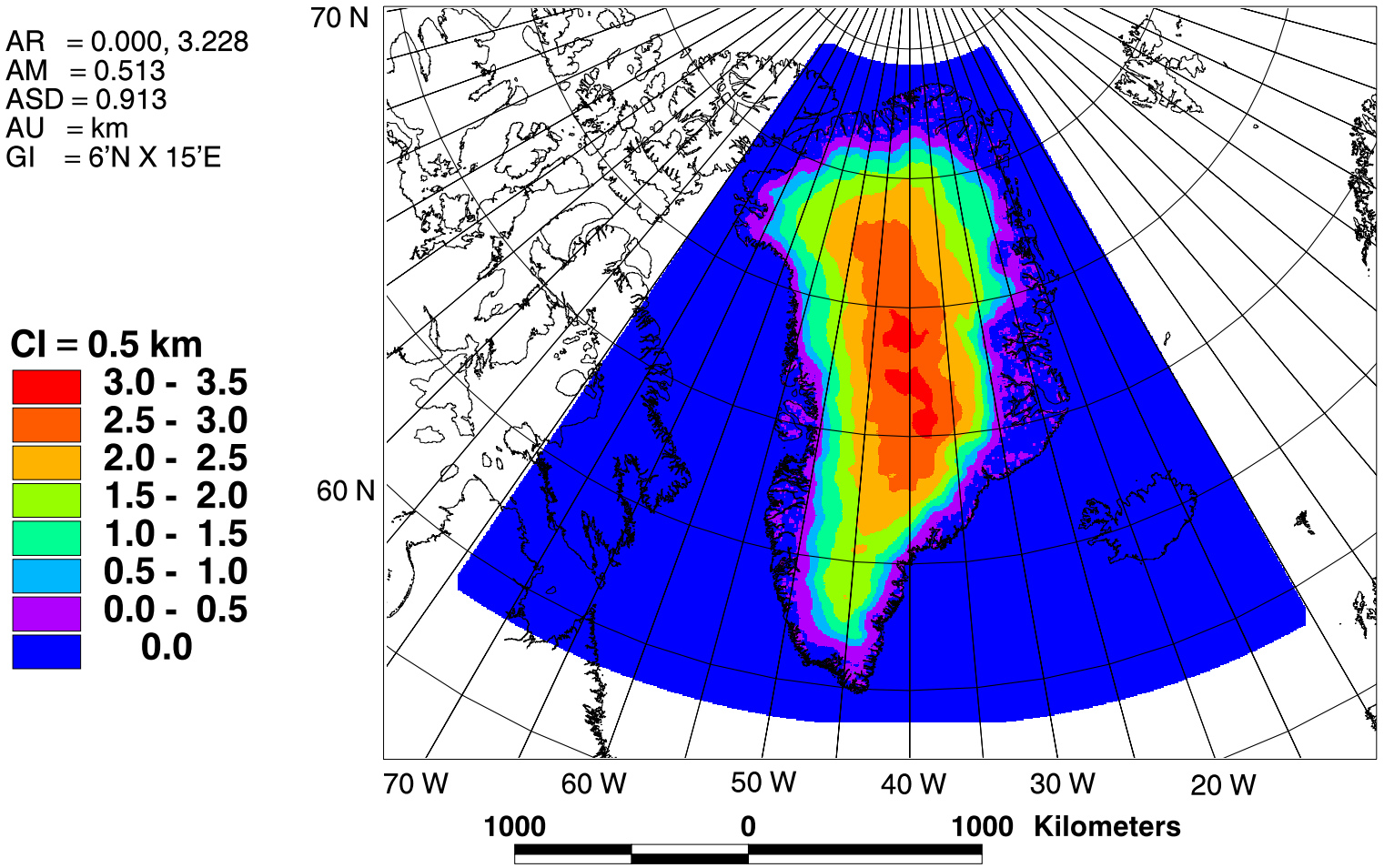

Figure 3.3: Ice thickness model (top minus bottom of icesheet) in a Lambert Equal-Area Azimuthal Projection centered on 40° W.

to lose track. Additionally, the coverage extended only to 72°N that was the limits of GEOSAT/SEASAT coverage. Thus, the surface grid from Ekholm [1996], which extends to the northern limits of Greenland (83°N), was used for this analysis.

3.3.2 Bedrock and Ocean Thickness DEMs

Oceanic (Figure 3.4) and rock (Figure 3.5) DEMs were derived from bathymetry estimated by the Gravity-Geologic Method (GGM) [Nagarajan, 1994]. This bathymetry represented a 54% improvement over JGP95E and 62% improvement over ETOPO5U when compared to over 250,000 control depths about Greenland [Chapter 2]. The northern extent of the GGM-derived bathymetry was limited to 80°N. North of 80°N, values from JGP95E, shown in Figure 2.20, were used because they compared most closely to the previously studied control points.

The bathymetry estimates provided complete coverage for the ocean DEM but did not cover regions above sea level nor beneath the Greenland icesheet. Elevations from Figure 3.2 were used for all areas onshore for Greenland and values from JGP95E were used for other areas above sea level in the study region. These three data sets (Figures 3.3, 3.4, and 3.5) then provided boundaries for estimating the terrain variations and the related TGE.

3.3.3 Free-Air Gravity Anomalies (FAGA)

Figure 3.7 shows the FAGA obtained from NIMA that were derived from surface, marine and airborne gravity observations by various agencies. These FAGA were calculated using least squares collocation on a 5' grid along with error estimates that are given in Figure 3.8. However, the predictions were not made at a uniform elevation, but rather upon the surface of a DEM defined by NIMA in Figure 3.9. This surface DEM is very similar to that of Ekholm [1996] in Figure 3.1. The FAGA

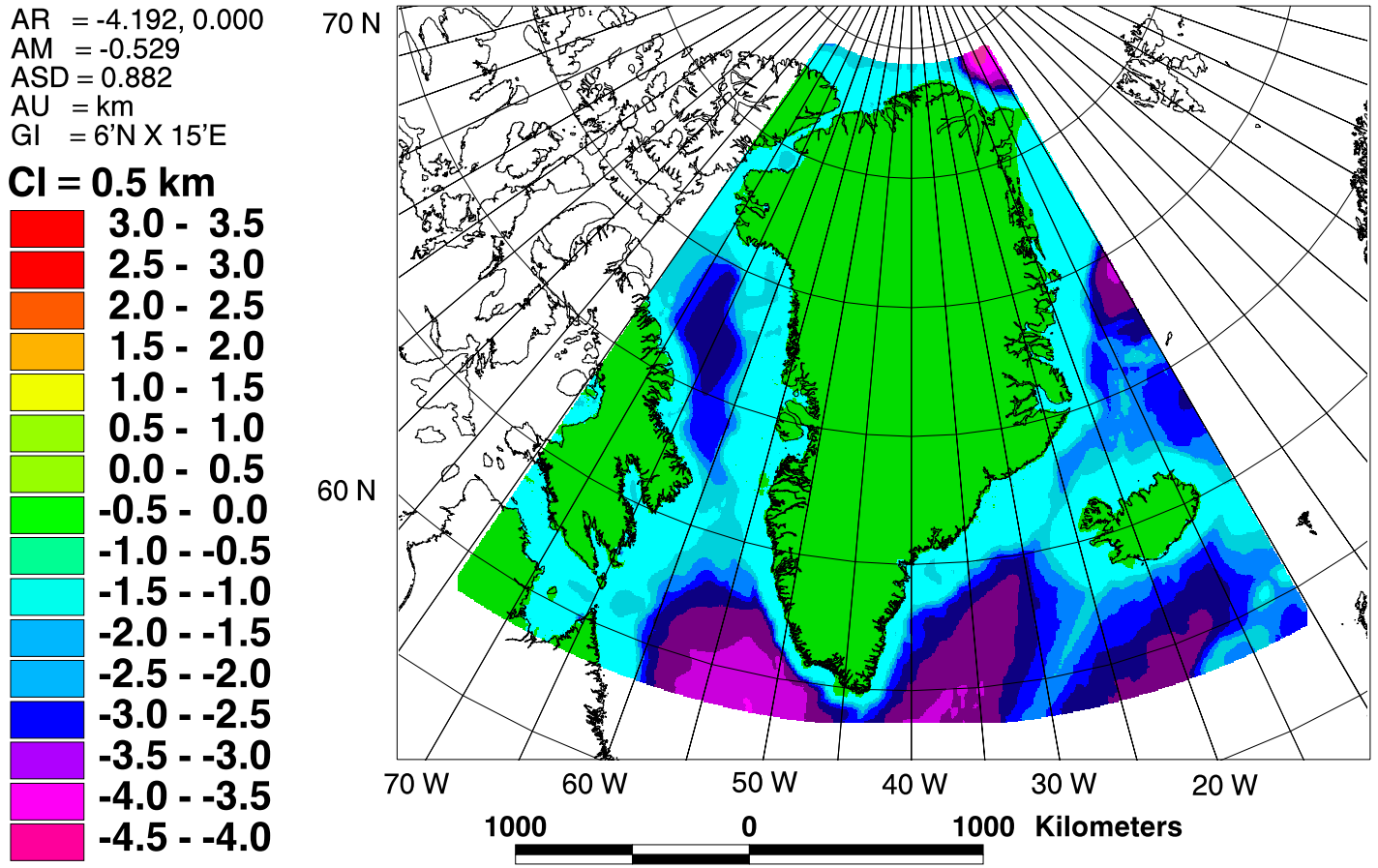

Figure 3.4: Ocean thickness model for Greenland (reference is MSL) in a Lambert Equal-Area Azimuthal Projection centered on 40° W.

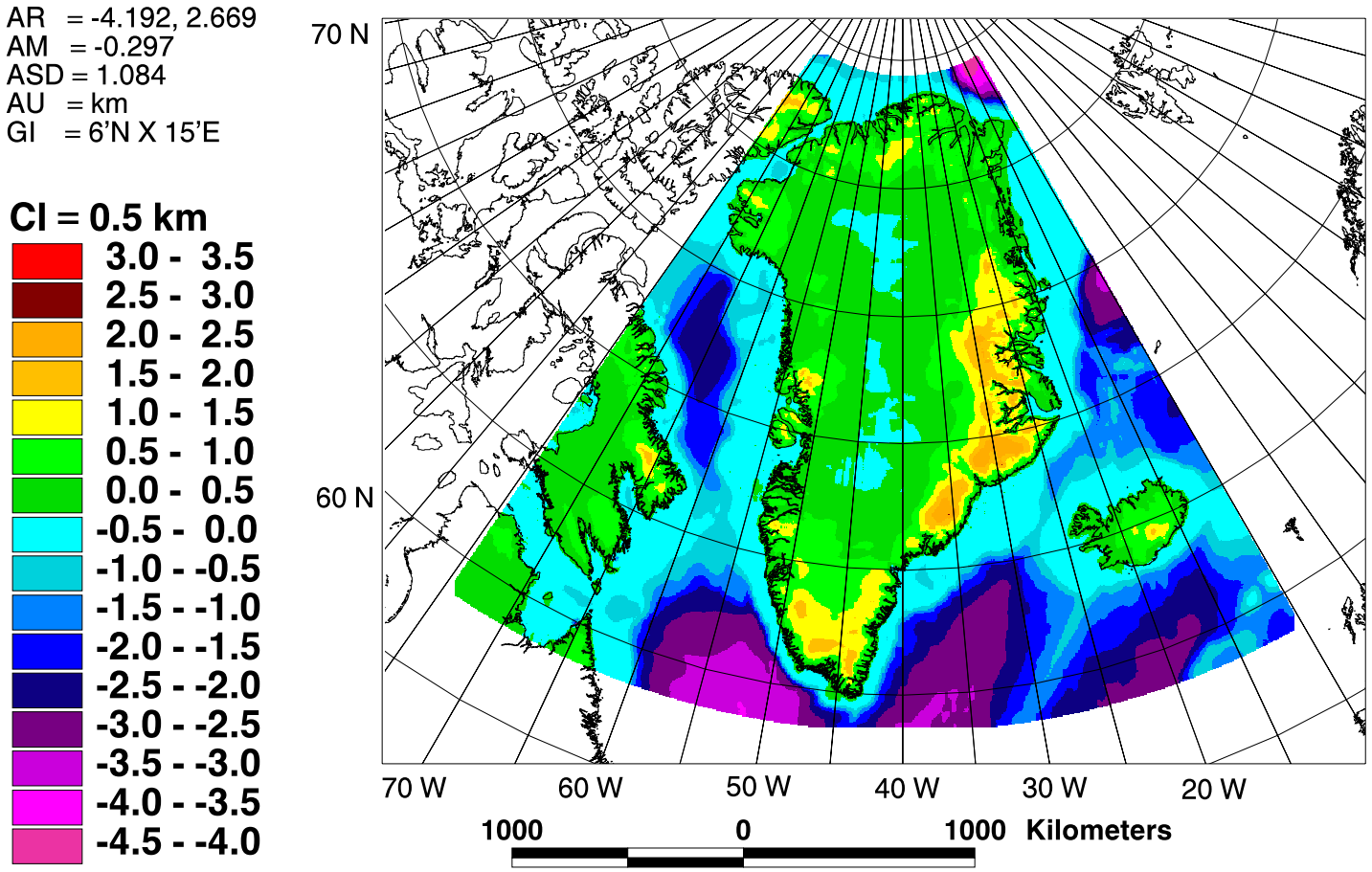

Figure 3.5: Bedrock surface model for Greenland (reference is MSL) in a Lambert Equal-Area Azimuthal Projection centered on 40° W.

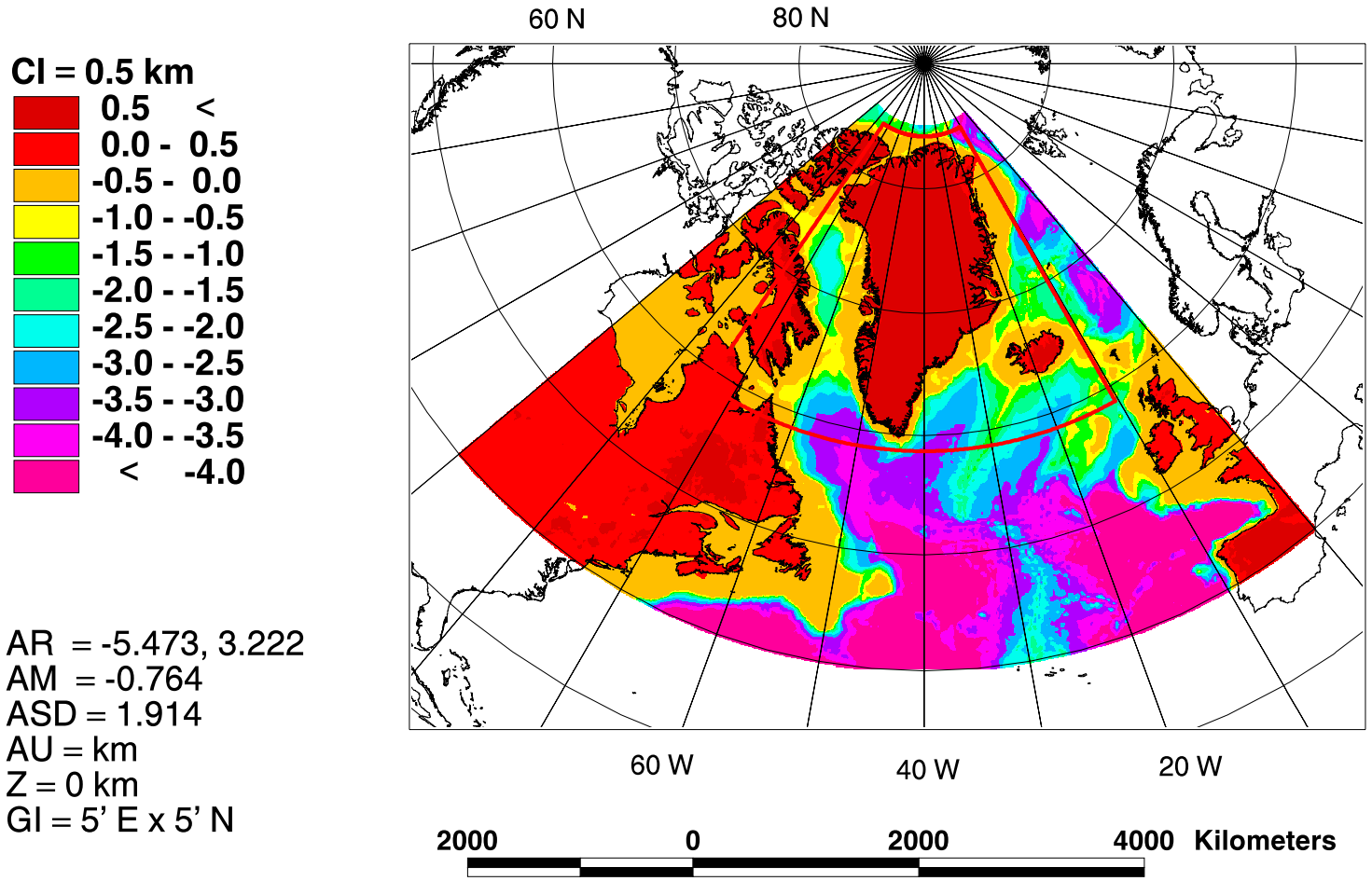

Figure 3.6: Greenland bathymetry from JGP95E data set in a Lambert Equal-Area Azimuthal Projection centered on 40° W.

were upward continued to a uniform elevation of 20-km as shown in Figure 3.10 for comparison with the TGE.

Additionally, FAGA for the interior of Greenland were derived primarily from the Greenland Aerogeophysical Projects of 1991 and 1992 [Brozena, 1995]. These data have a nominal track spacing of about 30 km, while FAGA from other surveys had a slightly better between track resolution. Therefore, upward continuation to 20-km does not significantly attenuate anomaly details, because of the fundamental lack of reliable signals below 20-km wavelength. The 20-km wavelength corresponds to a 10 km data interval or about 6' in latitude and 15' in longitude in the field area. Appendix A gives further details for the pre-processing of these gravity data and the generation of the 20-km upward continued FAGA that were used for this study.

To check the quality of the FAGA and the ice thickness, ocean, and rock DEMs, as well locating possible errors, the data sets are compared next with independent data from profiles along the 2000 m contour of Greenland collected by Byrd Polar Research Center (BPRC).

3.4 Comparison of Gridded Data Sets

During the 1995 and 1996 field seasons in Greenland, gravity and positional coordinates were obtained with a LaCoste-Romberg gravimeter and various GPS receivers [Roman et al., 1998] along the 2000 m contour around the Greenland ice cap (Figure 3.11). Additionally, unpublished ice thickness measurements were obtained by Siva Prasad Gogineni in 1997 beneath some of these gravity stations using airborne radar sensors. The resulting data are summarized in Appendix D and can be used to generate a profile around Greenland to check the quality of the NIMA FAGA (Figures 3.7), ice thickness (Figures 3.3), and surface elevation (Figure 3.1) DEMs

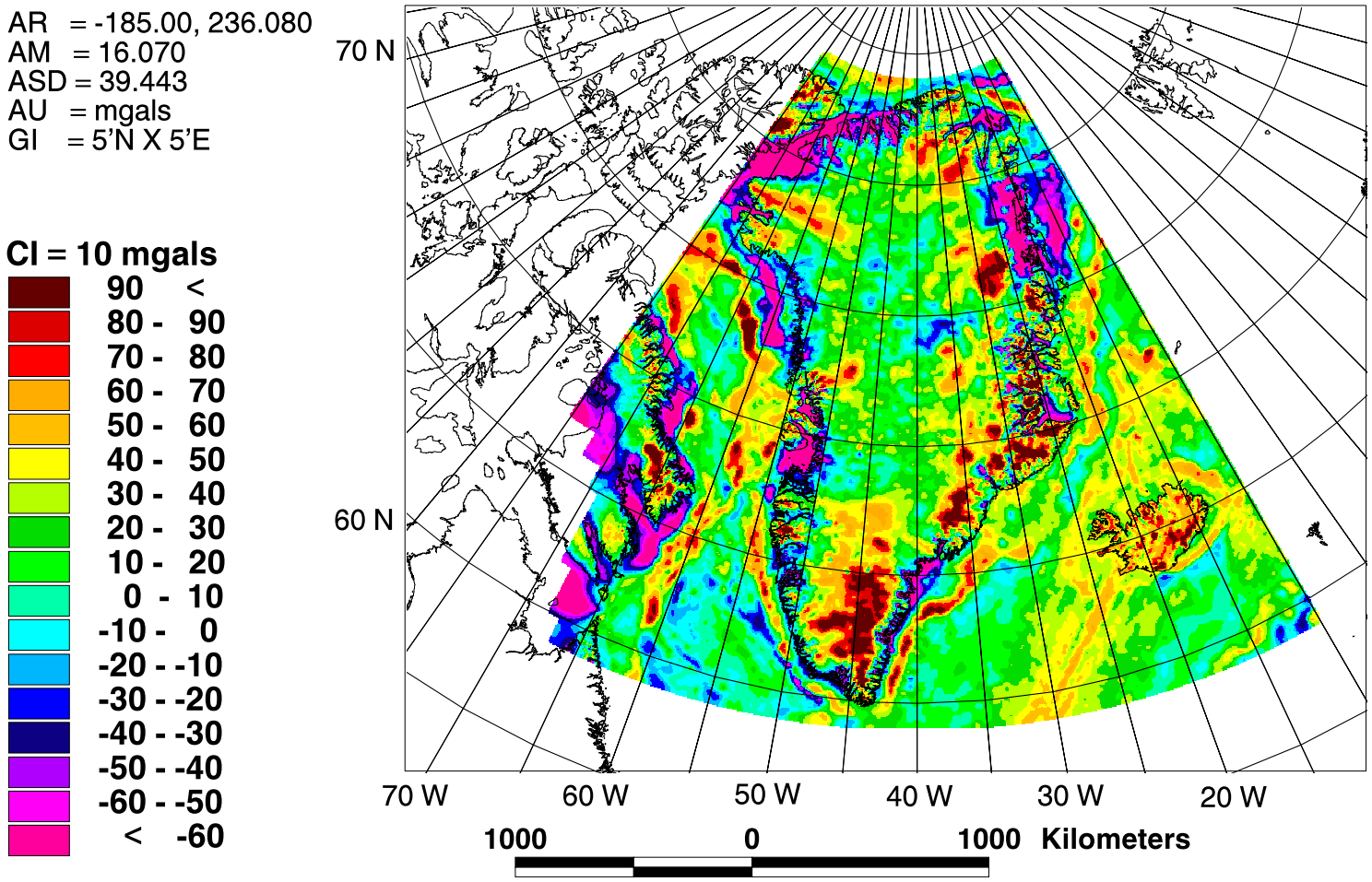

Figure 3.7: Original Free-Air Gravity Anomalies (FAGA) from NIMA at the Earth's surface in a Lambert Equal-Area Azimuthal Projection centered on 40° W. Data are registered to variable surface elevations that are given in Figure 3.9.

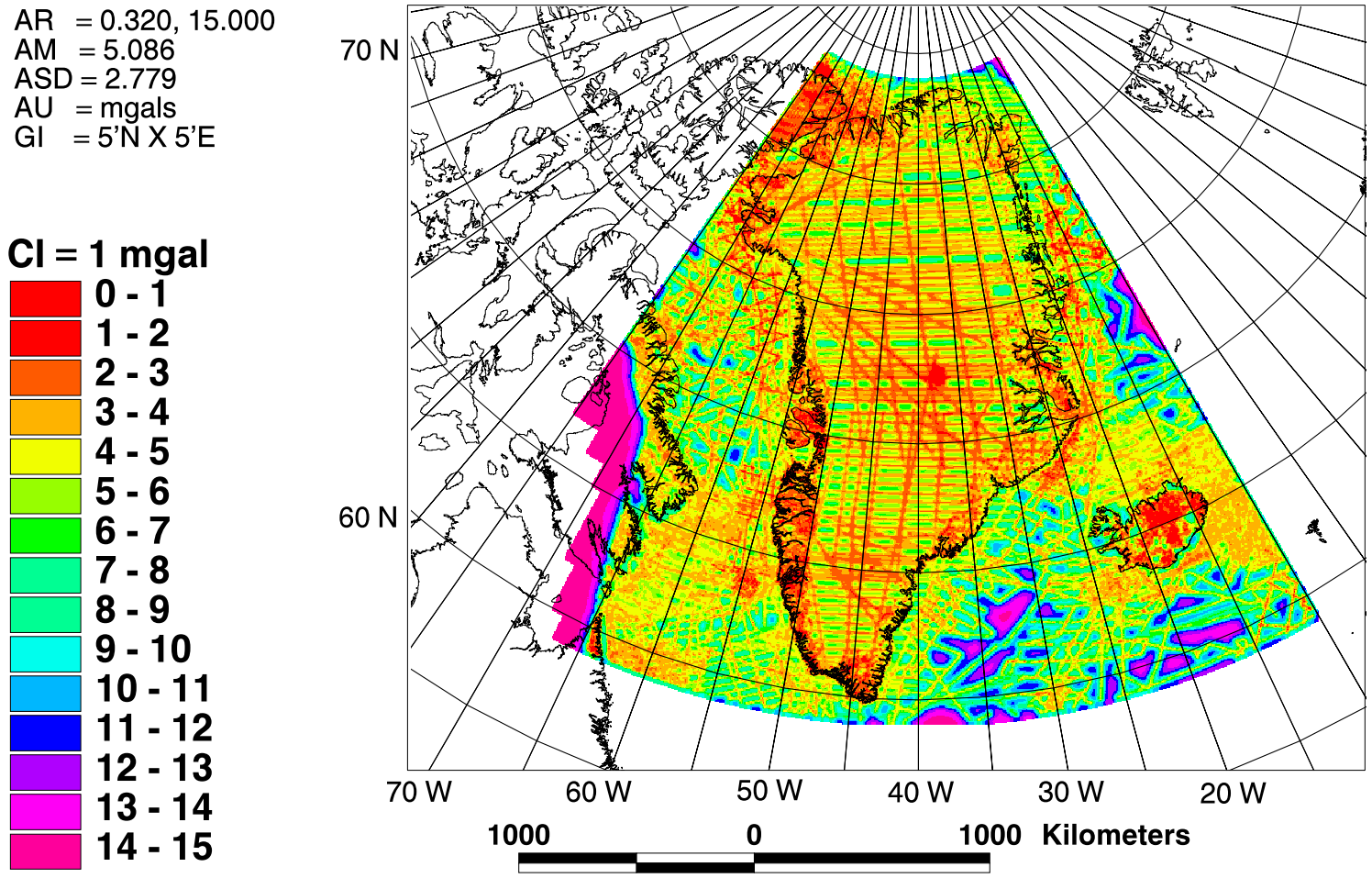

Figure 3.8: Observation errors provided with the NIMA FAGA in a Lambert Equal-Area Azimuthal Projection centered on 40° W.

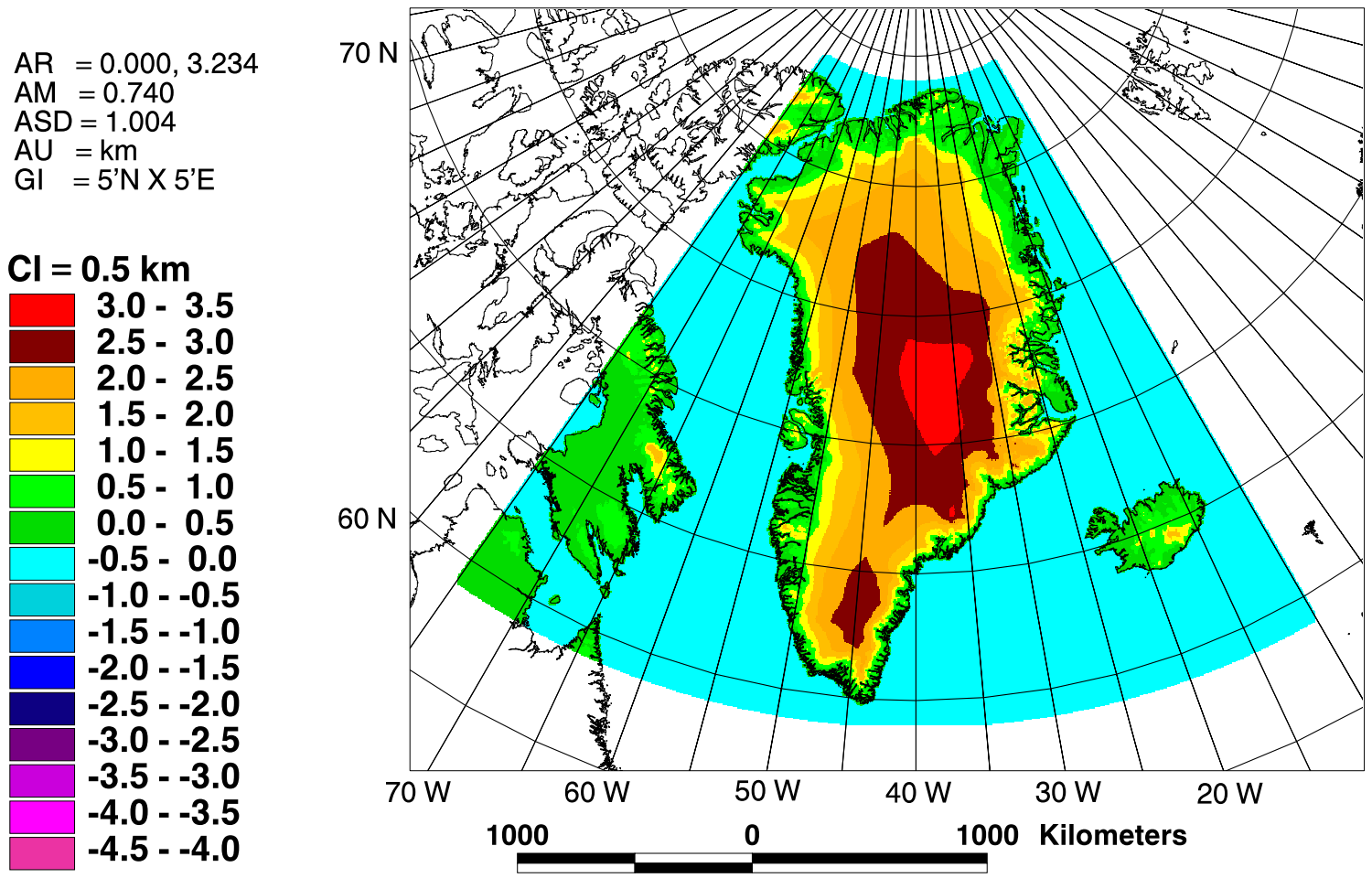

Figure 3.9: Orthometric heights associated with the NIMA's FAGA above mean sea level in a Lambert Equal-Area Azimuthal Projection centered on 40° W.

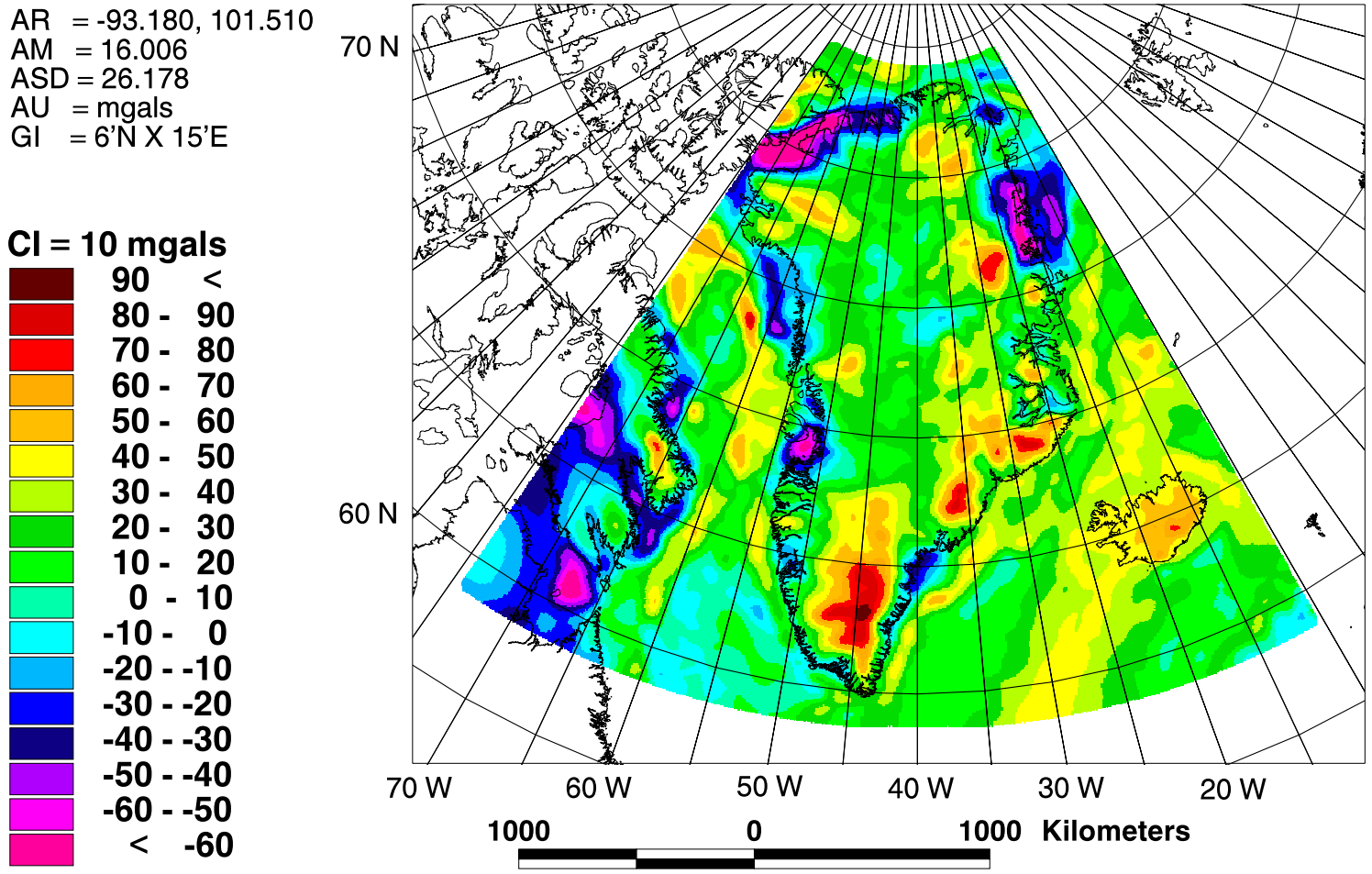

Figure 3.10: NIMA FAGA upward continued to Z=20-km elevation in a Lambert Equal-Area Azimuthal Projection centered on 40° W.

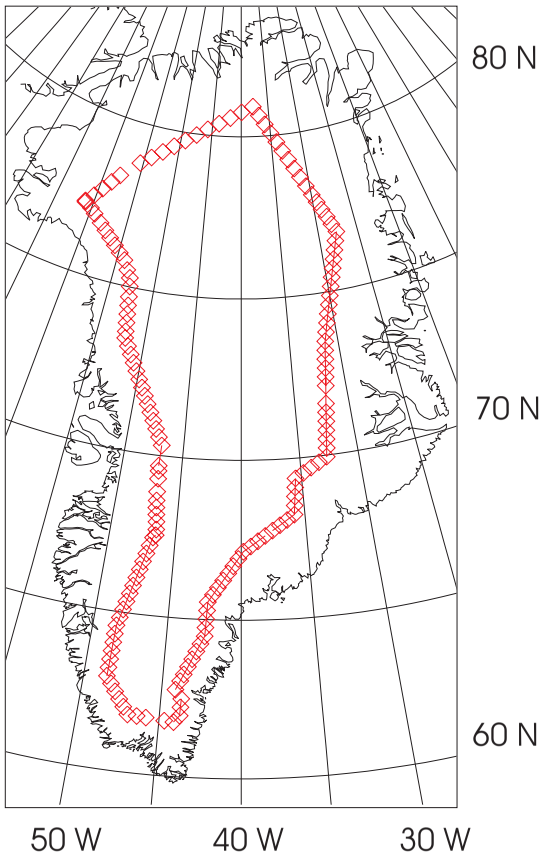

Figure 3.11: Greenland gravity and ice thickness measurement locations at about a 30 km interval gathered by Byrd Polar Research Center in 1992, 1993, 1995, and 1996 [Roman et al., 1998]. Data are shown in a Lambert Equal-Area Azimuthal Projection centered on 40° W.

The FAGA observations, positional coordinates, and ice thickness measurements are summarized for 159 BPRC data points in Table D.1. Additionally, EGM96 [Lemoine et al., 1997; 1998a; 1998b] geoid undulations were used to convert the ellipsoidal coordinates of each BPRC point to orthometric heights for comparison with the surface elevations from Ekholm [1996]. Table D.2 shows the values at the BPRC locations derived by interpolating the ice surface (Figure 3.1), ice bottom (Figure 3.2), ice thickness (Figure 3.3), NIMA height grid (Figure 3.9), and original NIMA FAGA grid (Figure 3.7).

Comparison of these profiles with the interpolated data will provide valuable insights into the quality of all data. Areas of agreement may be assumed to validate both data sets in a region. Determination of errors and their impact on the final predictions also aid in assessing the quality of the final Moho depth predictions.

3.4.1 Surface Elevation Comparison

The elevation data obtained from Ekholm [1996] will be used for determining the top of the ice mass for the Moho depth predictions. An estimate of the quality of these data would be useful for evaluating the quality of the TGE and related Moho depth predictions. Accordingly, the Ekholm [1996] data were compared with the NIMA DEM and BPRC elevation profiles, which are assumed to represent the truest elevations because they were *in situ* measurements.

The NIMA heights reflect the elevation at the nodes where the NIMA FAGA were provided. These data were linearly interpolated to the locations of the BPRC points to provide the NIMA ice surface values (Table D.2). Similarly, the Ekholm [1996] data were interpolated to generate values at the BPRC locations (Table D.2). In Figure 3.12, the BPRC data are compared to ice surface data interpolated from the NIMA DEM (Figure 3.9) and the Ekholm [1996] DEM (Figure 3.1).

Comparison Made	CC (%)	Difference RMS (m)	mean (m)	max. (m)
BPRC vs. Ekholm	99.8	20.5	-1.5	72.6
BPRC vs. NIMA	99.8	20.9	0.1	84.5
Ekholm vs. NIMA	100.0	7.0	1.7	52.8

Table 3.1: Statistical Comparison of Ice Surface Elevation Data. Surface elevation data from the BPRC profiles and interpolated values from Ekholm [1996] and NIMA DEMs are compared. All three profiles are very similar with the interpolated Ekholm and NIMA grids being almost identical. Columns listed compare the pairs of profiles, giving their correlation, the RMS of their difference, the mean of their difference, and the maximum value of the difference. All heights are orthometric (above the geoid). EGM96-determined geoid undulations were removed from the ellipsoidal heights of the BPRC data.

The 3 profiles are nearly coincident as shown in Figure 3.12.a. Examination of the differences in Figure 3.12.b reveals that the three profiles are nearly the same except for regions around the 2000 and 3500 km points along the profile. Table 3.1 demonstrates that the Ekholm [1996] data were marginally better than the NIMA DEM based upon the comparison with the BPRC data. Based upon this comparison, the Ekholm data were ultimately selected to represent the ice surface. The maximum difference of 72.6 m would be negligible in the gravity signal for the ice mass at 20-km elevation. Therefore, if this maximum value is assumed to be representative of the worst errors possible for the surface data, then these errors may be neglected.

Although the Ekholm [1996] DEM was selected for the ice surface in calculating TGE, the difference between the Ekholm [1996] and NIMA DEMs are relatively small at the interpolated BPRC points. Their RMS value is only 7 meters, indicating that 99% of the points for both DEMs were within 21 meters of each other. For all practical purposes, these two DEMs may be treated as identical.

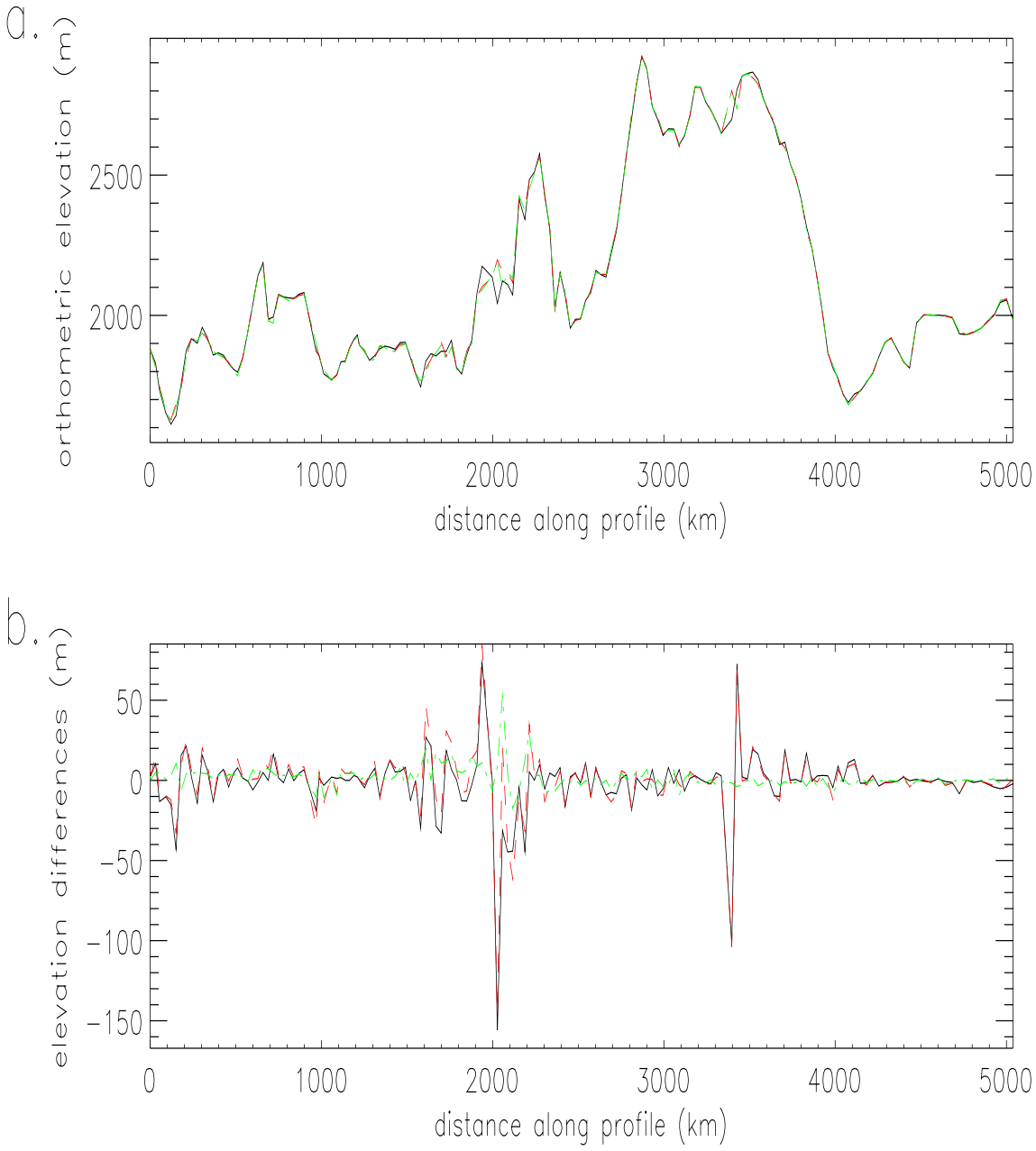

Figure 3.12: Ice Surface Elevation Comparisons. **a.** Orthometric heights given include: BPRC elevations (thickened black), Ekholm elevations (dashed red), and NIMA elevations (dashed green). **b.** Elevation differences given include: BPRC-Ekholm (thickened black), BPRC-NIMA (dashed red), and Ekholm-NIMA (dashed green). Table 3.1 gives statistics of this comparison.

3.4.2 Ice Thickness Comparison

In Figure 3.13 are shown profiles of the ice thicknesses interpolated from Figure 3.3 and those derived from the radar data, which are given in Table D.1. The radar-derived ice thickness data from Gogineni [Sohn and Csathó, 1998] extend only in 2 segments (thin-black line), and do not cover the entire length of the profile (thick-red line). The first segment compares favorably, but the large discrepancies (500 m) at the end of the second segment (to the right in Figure 3.13) are evident. Brozena [1995] described the subglacial model (Figure 3.2) as being derived from only 2 radar profiles in the northern region. The more recent radar measurements made by Gogineni have been checked to ensure their accuracy [pers. comm. Csathó, 1998]. Therefore, it is assumed that the ice model generated by differencing the Ekholm surface and subglacial models may be flawed by about 500 m, especially towards the north. Hence gravity estimates for the ice and rock masses that are based on the location of the subglacial surface would also be in error by a related amount. However, the gravity effect of this potential error is small when compared to the gravity effect of an average regional crustal thickness of 30-50 km. Also, the effects of this possibly erroneous mass assignment are further mitigated by the calculation of the TGE at 20-km elevation. Finally, this model is the most comprehensive available, and hence it will be retained with its possible errors noted for further reference and examination.

3.4.3 Gravity Comparison

The BPRC elevation and location information were used to generate FAGA values along the profile. Normal gravity (γ) was calculated by using the GRS80 International Gravity Formula given by:

$$\gamma = 978032.7* \quad (1.0 + 0.0052790414 * sin^2(lat.) + 0.0000232718 * sin^4(lat.) \qquad (3.8)$$

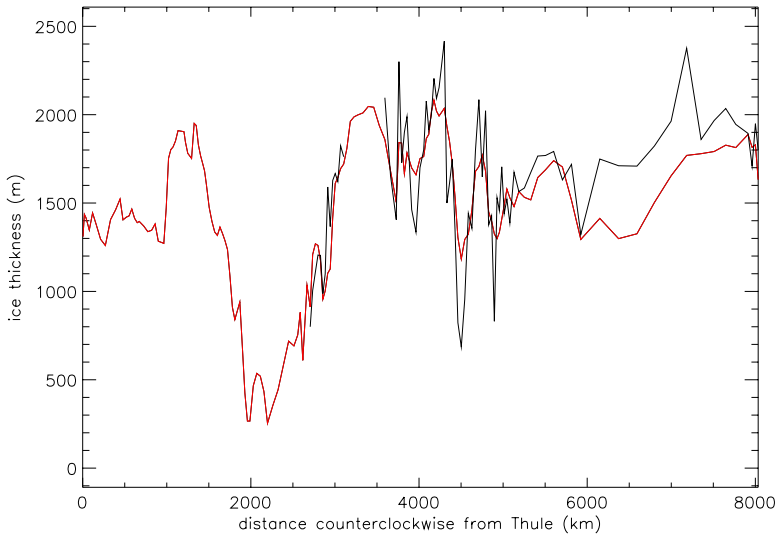

Figure 3.13: Comparison of ice thickness profiles showing data interpolated from Figure 3.3 (thick-red line) and the radar ice thickness measurements (two thin-black line segments) obtained by Gogineni and made available by Sohn and Csathó [1998].

$$+0.0000232718 * sin^4(lat.) + 0.0000001262 * sin^6(lat.)) \qquad mgals$$

An elevation correction of 0.3086 mgals/m was then applied using the GPS-derived ellipsoidal elevation to determine the γ value at the observation elevation.

It should be noted that the FAGA values were calculated at the ice surface and not on the geoid or at some uniform elevation. Additionally, these values were calculated by differencing the observed absolute gravity and normal gravity at the same elevation. Although these are more properly defined as gravity disturbances (cf. Heiskanen and Moritz [1967]), the original NIMA gravity data were similarly determined [Brozena, 1995; Forsberg and Kenyon, 1995], hence these two different data sets may be directly compared.

The principle difference between the NIMA and BPRC gravity values is that NIMA FAGA were determined for a 5' grid on a variable elevation surface (Figure 3.9).

Interpolating the NIMA DEM to the BPRC locations was shown to result in only a 0.1 m mean difference with a RMS difference of 20.9 m. Although the elevations interpolated from the NIMA DEM are not exactly the same as the BPRC elevations, they are sufficiently close that the differences in calculated FAGA over the elevation differences are negligible with respect to the observation errors associated with the NIMA FAGA (Figure 3.8), which have a mean of 5 mgals and range from 1 to 15 mgals.

The interpolated profile of NIMA FAGA is compared to the BPRC FAGA profile in Figure 3.14. These profiles start at Thule in northwest Greenland in the first entry of Table D.1. The profile continues down the west coast, around the southern end, up the east coast, and then along the north coast back to Thule. Only one major area of disagreement exists between the BPRC and NIMA FAGA profiles, which is located at the 2000 km interval along the X-axis in Figure 3.14 (in SW Greenland).

A cross-section showing the ice surface and bottom is shown in Figure 3.15 that demonstrates the ice thickness variations. Also plotted here is the difference (i.e., mismatch) between the gravity profiles shown in Figure 3.14. The large discrepancy in Figure 3.14 appears to be associated with significant glacial thinning starting at the 2000 km point and probably represents the increased gravity effect of the subglacial bedrock, which is closer to the surface in this region. Approximately 1.0 km of bedrock ($\Delta\rho$=2.74 gm/cm^3) displaces the ice ($\Delta\rho$=0.91 gm/cm^3) in this region, which is equivalent to a 77 mgal signal by the Bouguer Slab approximation given by:

$$g = 2\pi G \Delta\rho \Delta h \tag{3.9}$$

where: g = gravity effect of bedrock displacing ice;
G = gravitational constant = 6.672 mgals/[(gm/cm^3)*km];
$\Delta\rho$ = density contrast between the bedrock and ice
= 2.74 - 0.91 = 1.83 gm/cm^3; and
Δh = column height of rock displacing ice = 1 km

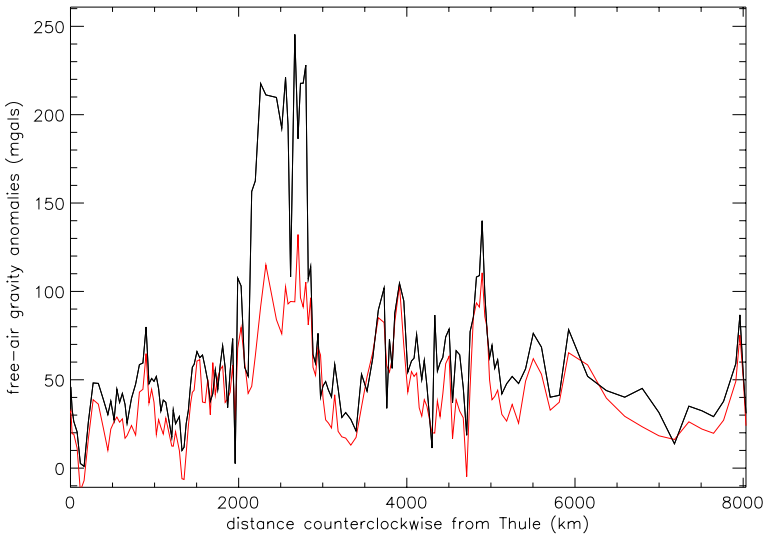

Figure 3.14: Comparison of FAGA profiles derived from BPRC field observations (thin-black line) and interpolated off the original NIMA FAGA grid (thick-red). Note the large disagreement at about the 2000 km point along the profile and that the NIMA FAGA are systematic lower in magnitude.

This is about the magnitude of the difference shown in Figure 3.15. Also noted in Figure 3.14 is the systematic difference between the NIMA FAGA and the profile derived from BPRC data. Since the NIMA FAGA are consistently lower in magnitude by about the same amount along the entire profile (i.e., biased), this will not affect the determination of Moho boundary undulations based on the use of the NIMA FAGA to modify the TGE. Hence, the grid of NIMA FAGA are assumed to be sufficiently similar to *in situ* measurements to be useful for calculating regional Moho depths.

3.5 TGE Determination by GLQ Integration

The terrain gravity effects (TGE) may be estimated from the summed gravity effects of the oceanic, rock, and ice masses using the related DEMs and appropriate densities by GLQ integration [von Frese et al., 1981; von Frese, 1980; Mateskon,

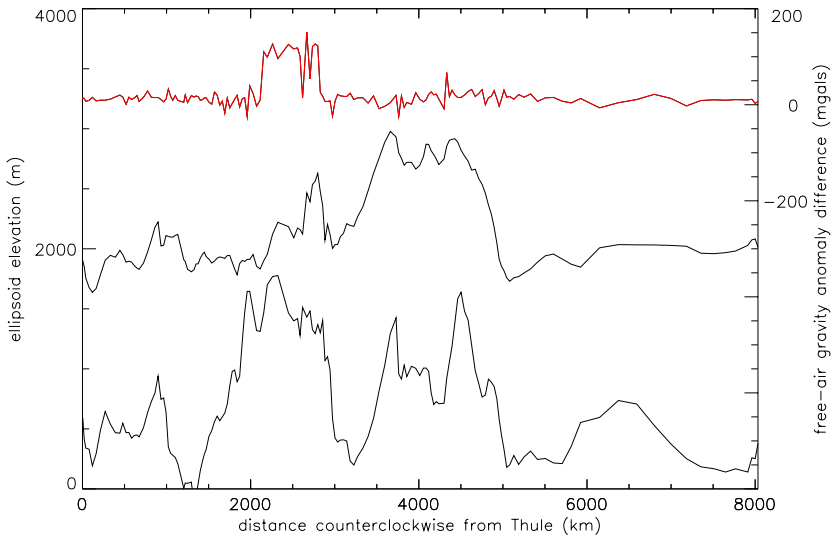

Figure 3.15: Crustal cross-section showing the ice top and bottom with FAGA differences. Top line shows the difference between BPRC-derived FAGA and NIMA-derived FAGA data. Middle line depicts the ice surface interpolated from Figure 3.1. The bottom line depicts the ice bottom interpolated from Figure 3.2. Note the large difference between the FAGA data sets that originates above a thinning of the ice sheet at the 2000 km point along the profile.

1985]. The gravity effects related to the ice and oceanic masses were determined using density contrasts that are always positive with respect to the air. For the effects of crustal rock, regions above a reference surface, such as mean sea level (MSL), were assigned positive density contrasts to approximate the effect of the rock mass that is displacing air above MSL. Conversely, for regions below the reference surface, negative density contrasts were assigned to approximate the gravity effect of rock mass that is missing between MSL and the bottom. A density contrast with respect to air of 0.9 gm/cm^3 was assumed for the entire iceload, and a density contrast of 1.03 gm/cm^3 was assumed for the ocean model. A more complex density model was used for the rock model.

Around the perimeter of Greenland, the slope break from the continental shelf to the oceanic abyssal plain was determined to occur at a depth of about 1000 m (Figures 2.18, 2.19, and 2.20). Some recent seismic studies [Chian and Louden, 1992; 1994; Fechner and Jokat, 1996; Gohl and Smithson, 1993; Jackson and Reid, 1994; Reid and Jackson, 1997] provide direct evidence of the location of this transition. Finally, Kerr [1980] indicated that most plate movement analyses used the 1000 m isobath to determine plate edges.

Based upon these analyses, regions shallower than 1000 m were assigned a density contrast of 2.74 gm/cm^3 and deeper regions were assigned 2.85 gm/cm^3. This *a priori* model is shown in Figure 3.16. A differential model for the lower crust was also used with values of 2.86 gm/cm^3 and 2.95 gm/cm^3 for the lower continental crust and lower oceanic crust, respectively. These density assumptions were made in an effort to model the increase in density with depth within a rock prism. The average continental crustal density was then 2.8 gm/cm^3 and the average oceanic crustal density was 2.9 gm/cm^3. Crustal density variations across the transitional crust were initially assumed to be negligible for the *a priori* model and adjusted to

account for the residual components of the gravity field resulting from the mismatch of the Moho depth model.

These contrasts were assumed for bodies defined by flat topped and bottomed prisms at intervals of 6'N and 15'E, which were the data intervals for all DEMs and the FAGA grid. For prisms with a positive DEM value (above MSL), the top was assigned the DEM value and the bottom was assigned to zero (MSL). For prisms with a negative DEM value (below MSL), the top was assigned to zero and the bottom to the DEM value. The modeling of the ice mass required DEMs to define the top (Figure 3.1) and bottom (Figure 3.2), because neither the ice surface or the subglacial surface could be referenced to a common level such as MSL. Therefore, both DEMs were needed to bound the prisms for calculating the TGE of ice by GLQ integration [Mateskon, 1985].

The gravity effects of the ice (Figure 3.17), ocean water (Figure 3.18) and rock (Figure 3.19) components of the crust were calculated using Equation 3.1 and are strongly correlated to their respective source grids (Figures 3.3, 3.4, and 3.5). The cumulative effect of these components at 20-km above MSL is the desired TGE (Figure 3.20), while the DEM of the Earth's surface is given in Figure 3.21.

3.6 Inversion for the Moho Depth Model by GLQ Integration

If an Airy model of isostatic compensation is assumed, then the component of FAGA at 20-km (Figure 3.10) that shows strong positive correlation (CC >0.76) or negative correlation (CC<-0.90) with the TGE may possibly reflect conditions of isostatic disequilibrium. Selection of threshold CC's greater than 0.76 or less than 0.90 was focused on minimizing the correlation of the retained FAGA with respect to the TGE (i.e., the remaining FAGA data were decorrelated with respect to the total TGE model).

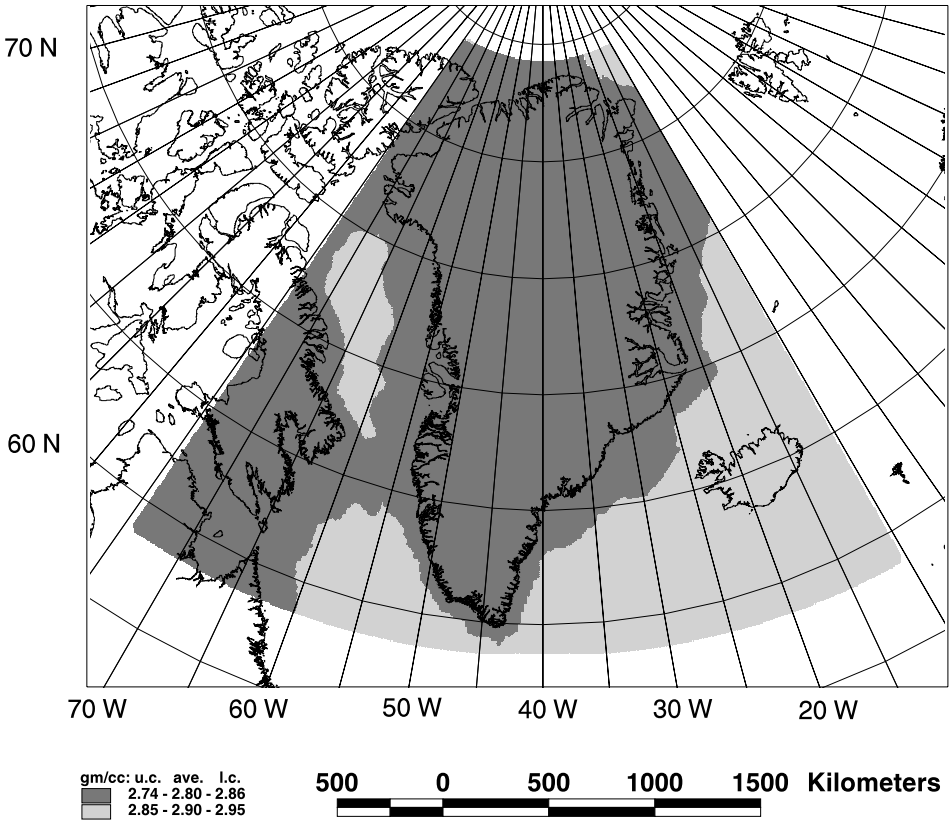

Figure 3.16: Initial assumed crustal densities for Greenland used in this study in a Lambert Equal-Area Azimuthal Projection centered on 40° W. Ranges of density values for prisms of oceanic and continental rock are given for the upper crust (u.c.), average for each prism (ave.), and lower crust (l.c.).

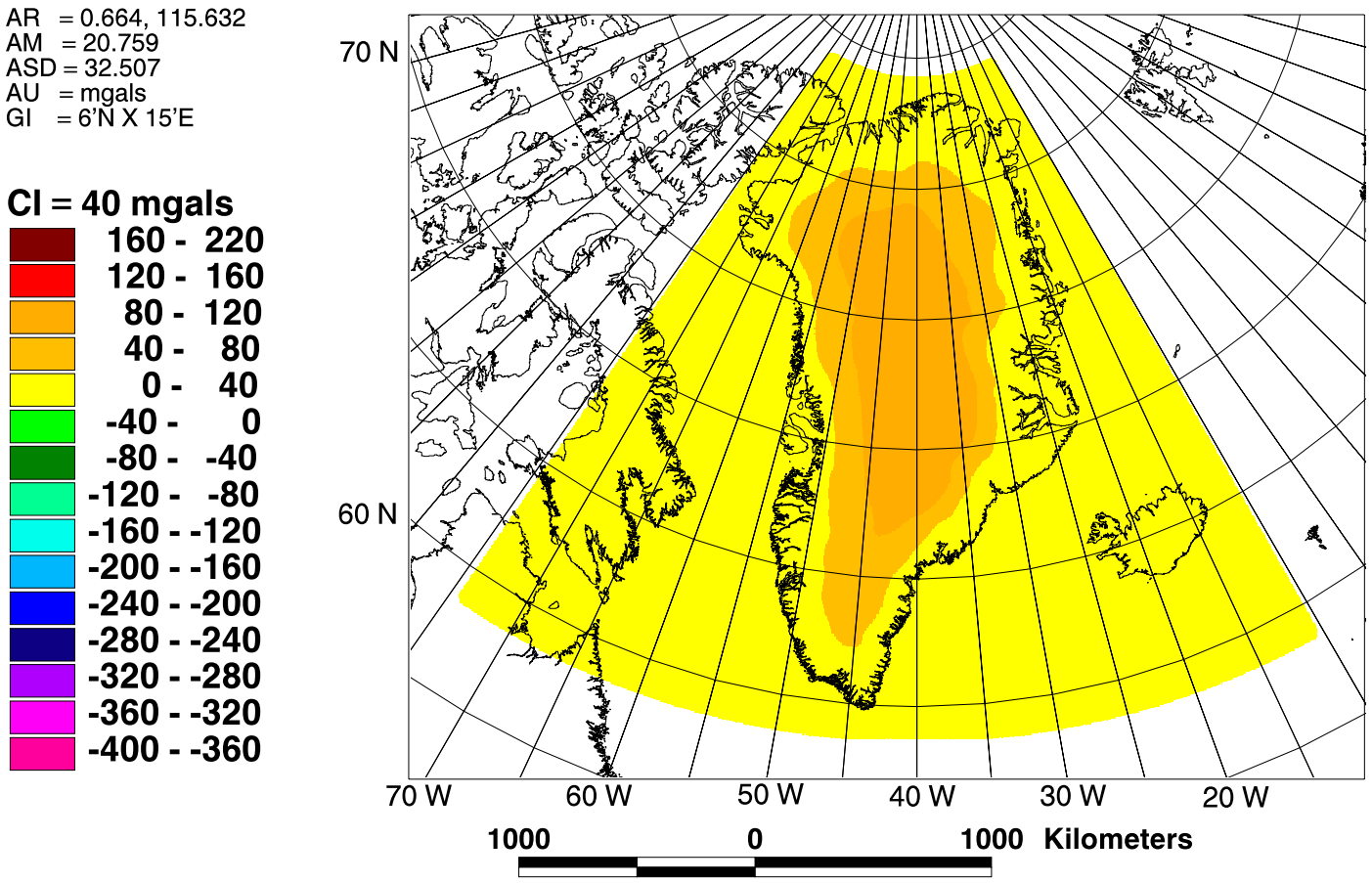

Figure 3.17: Gravity effect of the ice model at 20-km above MSL in a Lambert Equal-Area Azimuthal Projection centered on 40° W.